Short Communication:

Solvatochromism and Theoretical Studies of Dicyanobis(phenylpyridine)iridium(III) Complex Using Density Functional Theory

Noorshida Mohd Ali[1*], Anthony J.H.M. Meijer[2], Michael D. Ward[2,3], Norlinda Daud[1], Norhayati Hashim[1], and Illyas Md Isa[1]

[1]*Department of Chemistry, Faculty of Science and Mathematics, Universiti Pendidikan Sultan Idris, 35900, Tanjong Malim, Perak, Malaysia*

[2]*Department of Chemistry, University of Sheffield, Sheffield, S3 7HF, United Kingdom*

[3]*Department of Chemistry, University of Warwick, Coventry, CV4 7AL, United Kingdom*

**** Corresponding author:***

tel: +60-194484642
email: noorshida@fsmt.upsi.edu.my

Received: January 1, 2021
Accepted: February 11, 2021

DOI: 10.22146/ijc.62763

Abstract: *Luminescent cyanometallate $[Ir(ppy)_2(CN)_2]^-$ (ppy = $C_6H_5C_5H_4N$) has recently gained attention due to its desired photophysical properties. Our research group reported that the $[Ir(ppy)_2(CN)_2]^-$ has shown a negative solvatochromism like $[Ru(bipy)(CN)_4]^{2-}$, resulting in a blue-shift of the UV-Vis absorption bands in the water. Therefore, to gain insight into the specific solvent-solute interaction governed by the hydrogen bond in the solvation hydration shell, density functional theory (DFT) calculations were performed on the singlet ground state of the $[Ir(ppy)_2(CN)_2]^-$ and its solvent environment in the water at B3LYP level theory. It was demonstrated, seven water molecules provided a good description of the relevant spectra: IR and UV-Vis. The calculation reproduced the positions and intensities of the observed ν(C≡N) bands at 2069 and 2089 cm^{-1}. The calculated MLCT transition wavelength was 366 nm vs. a measured value of 358 nm, differing by 8 nm. The study revealed the water molecules interacted with cyanide ligands through CN···H–OH type hydrogen bonds and water-water interactions ($HO–H···OH_2$ type hydrogen bonds) were involved in the solvation hydration shell around the $[Ir(ppy)_2(CN)_2]^-$.*

Keywords: *iridium(III) anionic complex; DFT calculation; solvation hydration shell; cyanide ligand*

■ INTRODUCTION

The anionic complex $[Ir(ppy)_2(CN)_2]^-$ which is one of the general family of iridium(III) complexes based on cyclometallating phenylpyridine ligands, has attained eminence recently for its needed photophysical properties [1-4]. Luminescent cyanometallate $[Ir(ppy)_2(CN)_2]^-$ (Fig. 1) with two lone pairs on the cyanide ligands that was first reported in 2003 [5] and several derivatives [6] have shown a greater emissive and high energy excited state, and thus potentially good energy donors. Besides, these complexes can be used for direct coordination to a metal cation *via* the cyanide groups, in which they can be exploited in the field of supramolecular photochemistry, like $[Ru(bipy)(CN)_4]^{2-}$. Furthermore, the lone pairs on the N atoms of the cyanide ligands of $[Ir(ppy)_2(CN)_2]^-$ can form hydrogen bonds with protic solvent molecules that act as a hydrogen-bond donor, and hence allowing

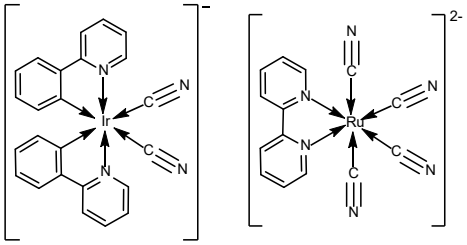

Fig 1. Structure of $[Ir(ppy)_2(CN)_2]^-$ (left) and $[Ru(bipy)(CN)_4]^{2-}$ (right)

the complexes to act as a component of hydrogen-bonded assemblies [7-9].

Our research group reported that $[Ir(ppy)_2(CN)_2]^-$ shows a negative solvatochromism, resulting in a blue-shift of the UV-Vis absorption bands in water concerning other solvents such as methanol, acetonitrile, dichloromethane, acetone, and dimethylformamide [3]. This solvatochromism arises in part due to the partial protonation of cyanide lone pair, which increases its π-acceptor ability and resulting in more significant Ir(dπ)→CN(π*) back bonding [8]. Therefore, it stabilizes the t_{2g} orbitals, giving a large energy difference between the highest occupied molecular orbital and the lowest unoccupied molecular orbital (HOMO-LUMO gap). Back donation from the filled *d*-orbitals on the Ir metal to the empty π*-orbitals of the CN^- ligand concerning M–C bond as indicated by the orbital diagram) is shown in Fig. 2. The results in a withdrawal of electronic charge from the metal center explain the blue shifts in metal to ligand charge transfer (MLCT) absorption band.

Since $[Ru(bipy)(CN)_4]^{2-}$ has been discovered to be used as a sensor for traces of moisture [8], it is projected that the solvatochromism of $[Ir(ppy)_2(CN)_2]^-$ will be in the same way as $[Ru(bipy)(CN)_4]^{2-}$ but possibly less due to the smaller number of cyanide ligands. Therefore, to get further information on the specific solvent-solute interaction governed by the hydrogen bond in the solvation hydration

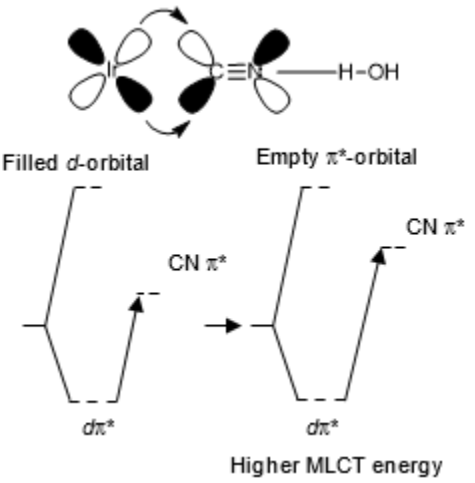

Fig 2. A presentation of π-donation of electron density from a filled metal orbital to the anti-bonding π* orbital of the CN^- ligand

shell, density functional theory (DFT) calculations have been carried out for the ground state of $[Ir(ppy)_2(CN)_2]^-$. Also, variations of the CN···H–OH hydrogen bonds of the singlet ground-state complex have been performed for $[Ir(ppy)_2(CN)_2]^-\cdot(H_2O)_n$.

■ COMPUTATIONAL METHODS

Theoretical studies were performed using the Gaussian 09, version C.01 program package [10] at the hybrid density functional theory (DFT) level. More precisely, Becke's three-parameter functional and the Lee-Yang-Parr functional (B3LYP) have been used throughout. In all calculations, an extensive basis set was used, consisting of 6-311G** [11–14] on all atoms (C, H, N, O) apart from iridium, which was described using a Stuttgart-Dresden pseudo-potential [15-18]. Besides, bulk solvent effects were treated *via* the polarizable continuum model (PCM) [19-22]. Finally, all calculations were run using ultrafine integrals, and no symmetry was considered in the calculations. During the optimization, each water was allowed to explore its configurational space completely freely [13,23]. In all cases where the converged structures were obtained, the frequencies within the harmonic approximation were calculated for use compared to the IR spectra. However, since B3LYP overestimates frequencies, these frequencies were scaled by 0.97 [24-25] to achieve better agreement with the experimental values. The converged species were also subsequently used in a TD-DFT calculation to obtain UV-Vis spectra. In each TD-DFT calculation, 100 states were included to get a spectrum down to approximately 250 nm. The electronic and vibrational spectra were analyzed using the *GaussSum* program.

■ RESULTS AND DISCUSSION

Calculated Structures

All DFT calculations were started from the $[Ir(ppy)_2(CN)_2]^-$ crystal structure, [3] which was optimized at the singlet ground state without any specific hydrogen-bonded interactions. A sequential process was implemented to model the solute-solvent interaction. First, a single water molecule (A) was selected to be coordinated linearly to the CN^- unit,

making a CN H angle of 180°. Then, another water molecule (B) was coordinated to the adjacent CN^- unit. Therefore, for the first solvation shell, two water molecules were included in the structure of $[Ir(ppy)_2(CN)_2]^-$ *via* CN···H–OH type hydrogen bonds. Fig. 3 shows that after minimization, the hydrogen bond distance between CN···H is approximate 1.9 Å, which is the typical length of a hydrogen bond [26]. However, the water molecules substantially altered from their original location. It can be seen that CN···H angles for both structures are in a range of 118–119°, which is not linear.

More water molecules were added in subsequent calculations until a total of seven water molecules surrounding the CN^- units were obtained. Notably, all the structures were converged in calculations. It was very challenging to measure a complete solvation shell model [13]. After minimization, the Ir–C distances in both ligands are calculated to be (2.065–2.071 Å) for the cyanide groups and (2.081–2.082 Å) for the phenylpyridine groups, which varied by –0.018 and +0.004 Å respectively, from the results in a vacuum. In contrast, the resulting Ir–N (2.102–2.100 Å) bond lengths differed by +0.020 Å from the results in a vacuum (Fig. 4). Significantly, there is no trend at all in bond lengths (Ir–C and Ir–N) with the increasing number of water molecules. The decrease in the distance between the Ir–C for cyanide ligands probably due to the added water molecules' presence, [13], from the arrangement of water molecules in the solvation shell (Fig. 4). It is evident that three water molecules were included for each CN^- ligand *via* CN···H–OH type hydrogen bonds. For instance, H_2O(B), H_2O(C), and H_2O(F) form hydrogen-bonded *via* CN···H–OH to one of the CN^- ligands. Besides, these two water molecules, H_2O(D) and H_2O(G), like a bridging ligand. Each of them is coordinated to the three adjacent water molecules [H_2O(A), H_2O(B) and H_2O(C)] and [H_2O(C), H_2O(E), and H_2O(F)], respectively *via* HO–H OH_2 type hydrogen bonds (Fig. 4). Consequently, the solvation shell around $[Ir(ppy)_2(CN)_2]^-$ involves both water molecules interacting with cyanide ligands and water-water interactions [13,23].

In all cases, the N O distances in the calculations (approximately 3.0 Å) with increasing numbers of water

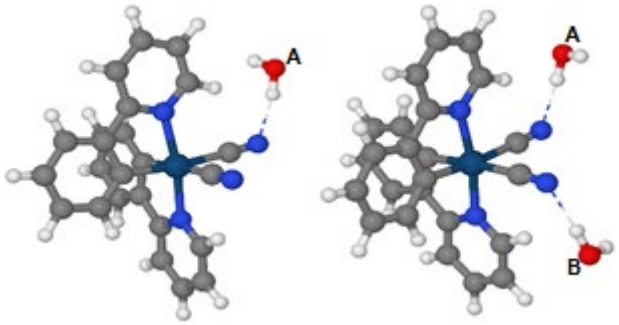

Fig 3. Calculated structures of $[Ir(ppy)_2(CN)_2]^-$ in water (PCM) solvent with one (left) and two (right) additional hydrogen-bonded water molecules included in the solvation shell

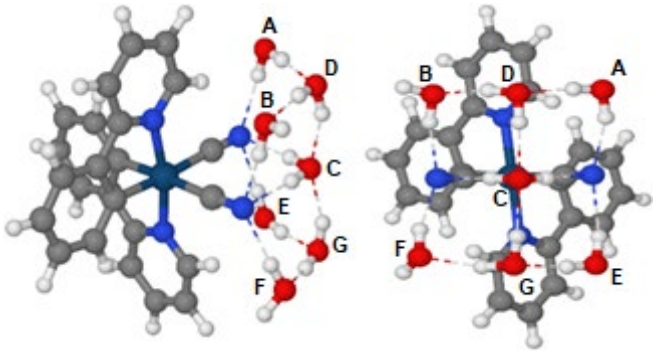

Fig 4. Calculated structures of $[Ir(ppy)_2(CN)_2]^-$ in water (PCM) solvent with seven additional hydrogen-bonded water molecules included in the solvation shell

molecules do not show any trends at all. They are slightly changed than those found in the earlier estimates on $[Ru(CN)_4(bipy)]^{2-}$ (approximately 2.9 Å) [23] and $[\{Ru(CN)_4\}_2(\mu\text{-bppz})]^{4-}$ (about 3.2 Å) [13]. In addition to the different types of ligands between ppy, bipy, and μ-bppz, the possible reason for this difference is that Horváth [23] study included one water molecule for each CN^- ligand then, another one water molecule was attached to the first one. The Meijer [13] reported only single water per CN^- ligand was included in the model.

Electrostatic Potential

To predict the behavior of the complex $[Ir(ppy)_2(CN)_2]^-$ with additional hydrogen-bonded molecules in the solvation shell, the electrostatic potential surface has been calculated. The electrostatic potential map in Fig. 5 clearly illustrates how the electrostatic potential changes around the

$[Ir(ppy)_2(CN)_2]^-$ without additional hydrogen-bonded water molecules in the solvation shell. Remarkably, it can be seen the most negative electrostatic potential (colored in shades of red) corresponds to a lone pair of CN^- ligands in the complex $[Ir(ppy)_2(CN)_2]^-$. This electron pair extends around the top of the CN^- unit, which will explain the deviation of the CN···H angle from 180°. Besides, the negative electrostatic potential is nearly cylindrical symmetrical around the CN triple bonds [13] and is relatively flat, so that deviations from linearity are easy to achieve.

Ground-state IR Spectra

Since the series of calculations $[Ir(ppy)_2(CN)_2]^-$ in water plus the solvation shell is consisting of one to seven hydrogen-bonded water molecules, all converged, it is possible to calculate the vibrational frequencies for all of them. The formation of the cyano-bridges in the $[Ir(ppy)_2(CN)_2]^-$ are proved by the C≡N stretching vibration bands in the range 2200–2000 cm^{-1} [27-28]. In the IR absorption spectrum of $[Ir(ppy)_2(CN)_2]^-$ in water, the characteristic band of the coordinated group with an intense peak is observed at 2085 cm^{-1}. The $[Ir(ppy)_2(CN)_2]^-$ in dichloromethane, however, displays two sharp ν(C≡N) bands at 2101 and 2092 cm^{-1} in the IR spectrum (Fig. S1). For $[Ir(ppy)_2(CN)_2]^-$ in water plus the solvation shell consisting of one hydrogen-bonded water molecule, the calculation reproduces the positions and intensities of the observed ν(C≡N) bands at 2102 and 2119 cm^{-1}. In contrast for $[Ir(ppy)_2(CN)_2]^-$ in water plus the solvation shell consisting of seven hydrogen-bonded water molecules, from the calculation, these two peaks are shifted to higher frequencies by approximately 30 cm^{-1} with the increased intensity (2069 and 2089 cm^{-1}) (Fig. 6). Therefore, the latter result shows a good agreement with the experimental data.

Absorption Spectra

In addition to the geometry minimizations, TD-DFT calculations for the optimized geometries with PCM approximation have been performed for the singlet ground state. The calculated electronic spectra for the $[Ir(ppy)_2(CN)_2]^-$ in water plus the solvation shell consisting of one to seven hydrogen-bonded water molecules are given in Fig. 7. In all cases, the absorption bands are shifted to a higher frequency with water molecules' addition and are very close to each other. The most extended wavelength peak can be described as an MLCT transition, as expected. It can be seen that the lowest-energy MLCT peak at 383 nm for one hydrogen-bonded water molecule is blue-shifted (366 nm) after addition with seven hydrogen-bonded water molecules.

Furthermore, weaker higher-energy MLCT should exist at 312 nm (one hydrogen-bonded water molecule) is shifted to a shorter wavelength (302 nm) after addition with seven hydrogen-bonded water molecules. Besides,

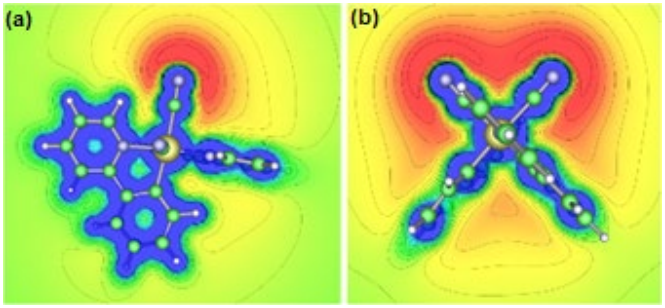

Fig 5. Electrostatic potential maps of $[Ir(ppy)_2(CN)_2]^-$ in two different planes. Panel (a): The plane is cutting through one of the CN^- units and perpendicular to the other CN^- unit Panel (b): The plane is cutting through both CN^- units

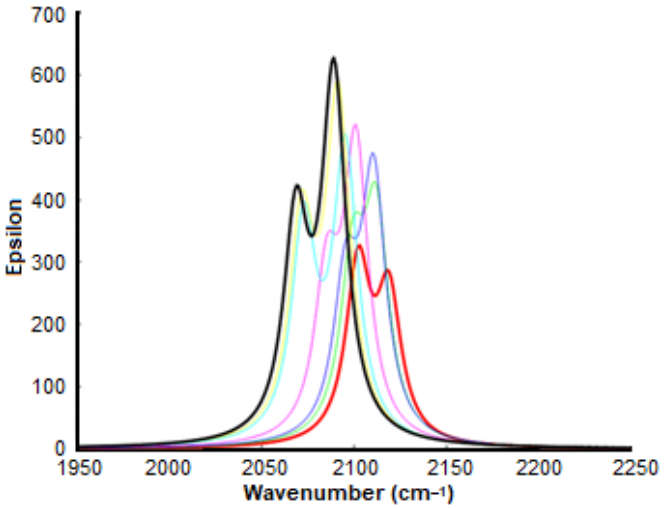

Fig 6. IR spectra of $[Ir(ppy)_2(CN)_2]^-$ in water with an additional water shell consisting of one (thick red line) until seven (thick black line) hydrogen-bonded water molecules, in the S_0 state. Line Half-width 8 cm^{-1}

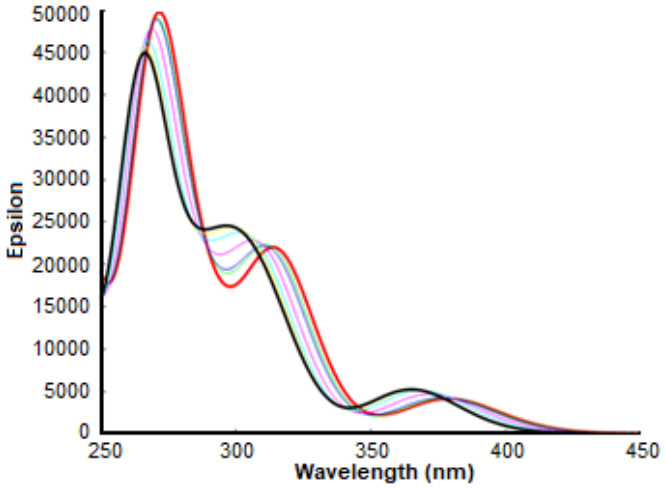

Fig 7. Calculated UV-Vis Spectra for $[Ir(ppy)_2(CN)_2]^-$ in water with an additional water shell consisting of one (thick red line) until seven (thick black line) hydrogen-bonded water molecules, Full-Width Half Maximum (FWHM) = 3000 cm^{-1}

Table 1. Detailed comparison of the singlet absorption spectrum between calculated and experiment for $[Ir(ppy)_2(CN)_2]^-$ in water with a water shell consisting of seven explicit hydrogen-bonded water molecules

Experimental wavelength (nm)	Calculated wavelength (nm)
358	366
290 (shoulder)	302
250	267

the higher energy π-π* transitions at 270 nm for one hydrogen-bonded water molecule is shifted slightly to higher energy (267 nm) with seven hydrogen-bonded water molecules. In particular, the higher energy π-π* transitions of 2-phenylpyridine is very little affected by the hydrogen bonding to the solvent with water molecules. It explains the solvatochromism behavior of this complex $[Ir(ppy)_2(CN)_2]^-$, in which the H-bond donating solvent molecules will interact with CN^- units [8]. Consequently, it is clear from the calculation that three transitions were get involved (Table 1). The contributions to these transitions show that the prominent peaks of the spectra are a combination of a blue shift ^{1}MLCT transitions from various Ir *d* orbitals to ppy ligands (as expected) and ^{1}π-π* transition on the ppy moiety [3,29-30].

Interestingly, a comparison of the calculated electronic spectrum for the $[Ir(ppy)_2(CN)_2]^-$ in water plus the solvation shell consisting of seven hydrogen-bonded water molecules with the experimental spectrum shows a satisfying agreement between theory and experiment (Fig. S2). Table 1 shows that the calculated wavelength with an additional water shell consisting of seven explicit hydrogen-bonded water molecules is 366 nm vs. a measured value of 358 nm, differing by 8 nm. The weaker higher-energy MLCT shoulder appears at 302 nm (calculated) vs. a measured value of 290 nm, differing by 12 nm. Therefore, it can be concluded that a description of the solvation shell with seven water molecules is good enough to model the specific solute-solvent interaction, as it gives a good fit with the electronic spectral data.

■ CONCLUSION

In conclusion, the structure of the anionic complex $[Ir(ppy)_2(CN)_2]^-$ and its solvent environment in water has been studied by DFT calculations. It has been demonstrated that seven water molecules create the hydration shell around the $[Ir(ppy)_2(CN)_2]^-$ providing a good description of IR and UV-Vis spectral data. In particular, three water molecules are localized near the nitrogen atom of each cyanide ligand. Besides, one water molecule is located between two adjacent water molecules at the center. Therefore, the solvation shell around $[Ir(ppy)_2(CN)_2]^-$ involves both water molecules interacting with cyanide ligands through CN···H–OH type hydrogen bonds and water-water interactions (HO–H···OH_2 type hydrogen bonds).

■ ACKNOWLEDGMENTS

The authors wish to thank the Research Management and Innovation Centre (RMIC), Universiti Pendidikan Sultan Idris (UPSI) for the University Research Grants (code: 2016-0184-101-01), and the University of Sheffield, the United Kingdom, for all affords and supports.

■ REFERENCES

[1] Lee, S., and Han, W.S., 2020, Cyclometalated Ir(III) complexes towards blue-emissive dopant for

organic light-emitting diodes: Fundamentals of photophysics and designing strategies, *Inorg. Chem. Front.*, 7 (12), 2396–2422.

[2] Ali, N.M., Ward, M.D., Hashim, N., and Daud, N., 2019, Synthesis and photophysical properties of bis(phenylpyridine) iridium(III) dicyanide complexes, *Mater. Res. Innovations*, 23 (3), 135–140.

[3] Ali, N.M., MacLeod, V.L., Jennison, P., Sazanovich, I.V., Hunter, C.A., Weinstein, J.A., and Ward, M.D., 2012, Luminescent cyanometallates based on phenylpyridine-Ir(III) units: solvatochromism, metallochromism, and energy-transfer in Ir/Ln and Ir/Re complexes, *Dalton Trans.*, 41 (8), 2408–2419.

[4] Pal, A.K., Henwood, A.F., Cordes, D.B., Slawin, A.M.Z., Samuel, I.D.W., and Zysman-Colman, E., 2017, Blue-to-green emitting neutral Ir(III) complexes bearing pentafluorosulfanyl groups: A combined experimental and theoretical study, *Inorg. Chem.*, 56 (13), 7533–7544.

[5] Nazeeruddin, M.K., Humphry-Baker, R., Berner, D., Rivier, S., Zuppiroli, L., and Grätzel, M., 2003, Highly phosphorescence iridium complexes and their application in organic light-emitting devices, *J. Am. Chem. Soc.*, 125 (29), 8790–8797.

[6] Sanner, R.D., Cherepy, N.J., and Young, V.G., 2016, Blue light emission from cyclometallated iridium(III) cyano complexes: Syntheses, crystal structures, and photophysical properties, *Inorg. Chim. Acta*, 440, 165–171.

[7] Martir, D.R., and Zysman-Colman, E., 2018, Supramolecular iridium(III) assemblies, *Coord. Chem. Rev.*, 364, 86–117.

[8] Ward, M.D., 2010, Structural and photophysical properties of luminescent cyanometallates $[M(diimine)(CN)_4]^{2-}$ and their supramolecular assemblies, *Dalton Trans.*, 39 (38), 8851–8867.

[9] Ahmad, H., Meijer, A.J.H.M., and Thomas, J.A., 2011, Tuning the excited state of photoactive building blocks for metal-templated self-assembly, *Chem.-Asian J.*, 6, 2339–2351.

[10] Frisch, M.J., Trucks, G.W., Schlegel, H.B., Scuseria, G.E., Robb, M.A., Cheeseman, J.R., Scalmani, G., Barone, V., Mennucci, B., Petersson, G.A., Nakatsuji, H., Caricato, M., Li, X., Hratchian, H.P., Izmaylov, A.F., Bloino, J., Zheng, G., Sonnenberg, J.L., Hada, M., Ehara, M., Toyota, K., Fukuda, R., Hasegawa, J., Ishida, M., Nakajima, T., Honda, Y., Kitao, O., Nakai, H., Vreven, T., Montgomery Jr., J.A., Peralta, J.E., Ogliaro, F., Bearpark, M., Heyd, J.J., Brothers, E., Kudin, K.N., Staroverov, V.N., Keith, T., Kobayashi, R., Normand, J., Raghavachari, K., Rendell, A., Burant, J.C., Iyengar, S.S., Tomasi, J., Cossi, M., Rega, N., Millam, J.M., Klene, M., Knox, J.E., Cross, J.B., Bakken, V., Adamo, C., Jaramillo, J., Gomperts, R., Stratmann, R.E., Yazyev, O., Austin, A.J., Cammi, R., Pomelli, C., Ochterski, J.W., Martin, R.L., Morokuma, K., Zakrzewski, V.G., Voth, G.A., Salvador, M.P., Dannenberg, J.J., Dapprich, S., Daniels, A.D., Farkas, O., Foresman, J.B., Ortiz, J.V., Cioslowski, J., and Fox, D.J., 2010, *Gaussian 09, Revision C.01*, Gaussian, Inc., Wallingford CT.

[11] Li, G.N., Zeng, Y.P., Li, K.X., Chen, H.H., Xie, H., Zhang, F.L. Chen, G.Y., and Niu, Z.G., 2016, Synthesis, characterization, properties and DFT calculations of 2-(benzo[b]thiophen-2-yl)pyridine-based iridium(III) complexes with different ancillary ligands, *J. Fluoresc.*, 26 (1), 323–331.

[12] Shang, X., Han, D., Zhan, Q., Zhang, G., and Li, D., 2014, DFT and TD-DFT study on the electronic structures and phosphorescent properties of a series of heteroleptic iridium(III) complexes, *Organometallics*, 33 (13), 3300–3308.

[13] Wragg, A.B., Derossi, S., Easun, T.L., George, M.W., Sun, X.Z., Hartl, F., Shelton, A.H., Meijer, A.J.H.M., and Ward, M.D., 2012, Solvent-dependent modulation of metal-metal electronic interactions in a dinuclear cyanoruthenate complex: A detailed electrochemical, spectroscopic and computational study, *Dalton Trans.*, 41 (34), 10354–10371.

[14] Grange, C.S., Meijer, A.J.H.M., and Ward, M.D., 2010, Trinuclear ruthenium dioxolene complexes based on the bridging ligand hexahydroxytriphenylene: Electrochemistry, spectroscopy, and near-infrared electrochromic

behaviour associated with a reversible seven-membered redox chain, *Dalton Trans.*, 39, 200–211.

[15] Demoin, D.W., Li, Y., Jurisson, S.S., and Deakyne, C.A., 2012, Method and basis set analysis of oxorhenium(V) complexes for theoretical calculations, *Comput. Theor. Chem.*, 997, 34–41.

[16] Li, L., Hu, J., Shi, X., Ruan, W., Luo, J., and Wei, X., 2016, Theoretical studies on structures, properties and dominant debromination pathways for selected polybrominated diphenyl ethers, *Int. J. Mol. Sci.*, 17 (6), 927.

[17] Latouche, C., Skouteris, D., Palazzetti, F., and Barone, V., 2015, TD-DFT Benchmark on inorganic Pt(II) and Ir(III) complexes, *J. Chem. Theory Comput.*, 11 (7), 3281–3289.

[18] Zhang, X., Jacquemin, D., Peng, Q., Shuai, Z., and Escudero, D., 2018, General approach to compute phosphorescent OLED efficiency, *J. Phys. Chem. C,* 122 (11), 6340–6347.

[19] Foxon, S.P., Green, C., Walker, M., Wragg, A., Adams, H., Weinstein, J.A., Parker, S.C., Meijer, A.J.H.M., and Thomas, J.A., 2012, Synthesis, characterization, and DNA binding properties of ruthenium(II) complexes containing the redox active ligand benzo[*i*]dipyrido[3,2-*a*:2',3'-*c*]phenazine-11,16-quinone, *Inorg. Chem.*, 51 (1), 463–471.

[20] Elliott, P.I.P., Haak, S., Meijer, A.J.H.M., Sunley, G.J., and Haynes, A., 2013, Reactivity of Ir(III) carbonyl complexes with water: Alternative by-product formation pathways in catalytic methanol carbonylation, *Dalton Trans.*, 42 (47), 16538–16546.

[21] Sahin, C., Goren, A., Demir, S., and Cavus, M.S., 2018, New amide based iridium(III) complexes: Synthesis, characterization, photoluminescence and DFT/TD-DFT studies, *New J. Chem.*, 42 (4), 2979–2988.

[22] Brahim, H., Haddad, B., Brahim, S., and Guendouzi, A., 2017, DFT/TDDFT computational study of the structural, electronic and optical properties of rhodium (III) and iridium (III) complexes based on tris-picolinate bidentate ligands, *J. Mol. Model.*, 23 (12), 344.

[23] Megyes, T., Schubert, G., Kovács, M., Radnai, T., Grósz, T., Bakó, I., Pápai, I., and Horváth, A., 2003, Structure and properties of the $[Ru(bpy)(CN)_4]^{2-}$ complex and its solvent environment: X-ray diffraction and density functional study, *J. Phys. Chem. A*, 107 (46), 9903–9909.

[24] Laury, M.L., Carlson, M.J., and Wilson, A.K., 2012, Vibrational frequency scale factors for density functional theory and the polarization consistent basis sets, *J. Comput. Chem.*, 33 (30), 2380–2387.

[25] De La Pierre, M., and Pouchan, C., 2018, Ab initio periodic modelling of the vibrational spectra of molecular crystals: The case of uracil, *Theor. Chem. Acc.*, 137 (2), 25.

[26] Desiraju, G.R., and Steiner, T., 2001, *The Weak Hydrogen Bond in Structural Chemistry and Biology*, International Union of Crystallography, Monographs on Crystallography, Oxford Science Publications, New York, USA.

[27] Smith, B.C., 2011, *Fundamentals of Fourier Transform Infrared Spectroscopy*, 2nd Ed., CRC Press, Boca Raton, USA.

[28] Nemec, I., Herchel, R., Šilha, T., and Trávníček, Z., 2014, Towards a better understanding of magnetic exchange mediated by hydrogen bonds in Mn(III)/Fe(III) salen-type supramolecular dimers, *Dalton Trans.,* 43 (41), 15602–15616.

[29] Pal, A.K., Nag, S., Ferreira, J.G., Brochery, V., La Ganga, G., Santoro, A., Serroni, S., Campagna, S., and Hanan, G.S., 2014, Red-emitting $[Ru(bpy)_2(N-N)]^{2+}$ photosensitizers: Emission from a ruthenium(II) to 2,2′-bipyridine ^{3}MLCT state in the presence of neutral ancillary "super donor" ligands, *Inorg. Chem*., 53 (3), 1679–1689.

[30] Pal, A.K., Cordes, D.B., Pringouri, K., Anwar, M.U., Slawin, A.M.Z., Rawson, J.M., and Zysman-Colman, E., 2016, Synthesis and characterization of green-to-yellow emissive Ir(III) complexes of pyridylbenzothiadiazine ligand, *J. Coord. Chem.*, 69 (11-13), 1924–1937.